OH Fragment from Benzoic Acid Monomer Photolysis: Threshold and Product State Distribution

Qiang Wei, Ju-Long Sun, Xian-Fang Yue, Shi-Bo Cheng, Can-Hua Zhou, Hong-Ming Yin,* and Ke-Li Han

State Key Laboratory of Molecular Reaction Dynamics, Dalian Institute of Chemical Physics, Chinese Academy of Sciences, Dalian 116023, China

Received: December 16, 2007; Revised Manuscript Received: February 29, 2008

Photodissociation dynamics of benzoic acid monomer (BAM) at different ultraviolet excitation wavelengths (280−295 nm) has been investigated. The nascent OH product state distributions were measured using the laser-induced fluorescence (LIF) technique. The rotational state distributions, the Λ-doublet-state ratio, and spin−orbit state distributions of the OH fragment were also measured at 280−294 nm. The OH fragments are vibrationally cold, and their rotational state distributions are peaked at $J'' = 3.5$ at each photolysis wavelength. No LIF signal of OH fragments was observed at 295 nm. The photodissociation threshold is determined to be 102.5−103.9 kcal/mol for OH channel. The dissociative state and mechanism have been discussed for OH produced from the photodissociation of BAM.

Introduction

Photodissociation of carboxylic acids in UV, which plays important roles in atmospheric, combustion, and interstellar chemistry, has been studied extensively.[1–17] Acetic acid has been studied at different wavelengths at 200,[4] 218,[5] 193,[6] and 193.3 nm[7] using the laser-induced fluorescence (LIF) technique. The results for the 218 and 200 nm photolysis of acetic acid provide strong experimental evidence for an exit channel barrier to produce $CH_3CO + OH$ from CH_3COOH. Kim[6] et al. and Naik[7] et al. have studied the photolysis of acetic acid at 193 and 193.3 nm, respectively. They found that the dissociation takes place indirectly along the triplet surface via curve crossing with the reverse barrier in the exit channel, and the observed energy partitioning is in excellent agreement with a hybrid model. By photolyzing acetic acid at different energies within its first electronic absorption band, they have made significant progress toward fully characterizing acetic acid's decomposition dynamics. Recently, Kumar and co-workers have studied the photodissociation dynamics of saturated[7,12–14] and unsaturated[15–17] carboxylic acids at different photolysis wavelengths. They observed an appreciable amount of energy being channeled into the relative translation of OH and its cofragment. Most of these acids undergo dissociation to produce OH fragments from the excited state with an exit barrier.[13,14,16,17]

Benzoic acid monomer (BAM) is the simplest member of the aromatic carboxylic acid family. A phenyl substitution may change the dissociation mechanism of aliphatic carboxylic acids, because of the conjugation interaction between the phenyl ring and the carboxylic group in aromatic carboxylic acids. Most of the work related to BAM is mainly focused on its electronic structure and spectra.[18–21] A few experimental and theoretical investigations have been performed to probe the decarboxylation mechanisms of BAM and its complexes with water.[22,23] In a recent work, Fang and co-workers[24] have mapped the potential energy surfaces of some low-lying excited states of BAM using CASSCF (complete active space self-consistent field) methods. They investigated the dissociation dynamics occurring on four different potential energy surfaces. They proposed that C−OH bond cleavage started from the T_2 state and led to the fragments of C_6H_5CO and OH, which was predicted to be the most possible channel upon photoexcitation of the BAM at 270 nm or shorter wavelengths.

In our previous letter, the photodissociation dynamics of BAM had been studied at 266 nm.[25] Considering the theoretic result,[24] we proposed that OH radical was mainly produced from BAM on the T_2 potential energy surface. However, there was lack of direct experimental evidence for OH producing exclusively from the T_2 state, and the possibility for OH producing from the S_1 state still existed. In the present paper, the photodissociation of BAM was studied at 280−295 nm. From the experimental results, we can not only identify the dissociative state but also verify the energy threshold for the OH fragment produced from the photodissociation of BAM.

Experimental Section

The experimental apparatus used in the present study has been described in detail elsewhere.[25–28] Here, we only give a brief description about our present experimental apparatus. The second-harmonic output (532 nm) of an Nd:YAG laser (Spectra-Physics, PRO-190) was used to pump a dye laser (Coherent, SCANMATE-PRO), which generated the wavelength-tunable laser pulses. The dye laser was operated using Rhodamine 6G dye and Rhodamine B dye, which the corresponding fundamental wavelength tuning ranges are 553−577 nm and 577−601 nm, respectively. The output of the dye laser was checked by a laser wavelength meter (Coherent) and then introduced into a harmonic generator (Coherent, Scanmate-SHG) to produce the frequency-doubled laser pulses, which were used for the photolysis laser pulses. The probe laser was another dye laser (Lumonics, HD-500) pumped by a second-harmonic output of Nd:YAG laser (Spectra-Physics, GCR-170). This dye laser was operated using DCM dye with a fundamental wavelength tuning range of 600−640 nm. The output of the dye laser was then introduced into a harmonic generator (Lumonics, HT-1000) to

* Corresponding author. Fax: +86 411 84675584. E-mail: hm_yin@dicp.ac.cn.

10.1021/jp711806u CCC: $40.75
Published on Web 05/06/2008

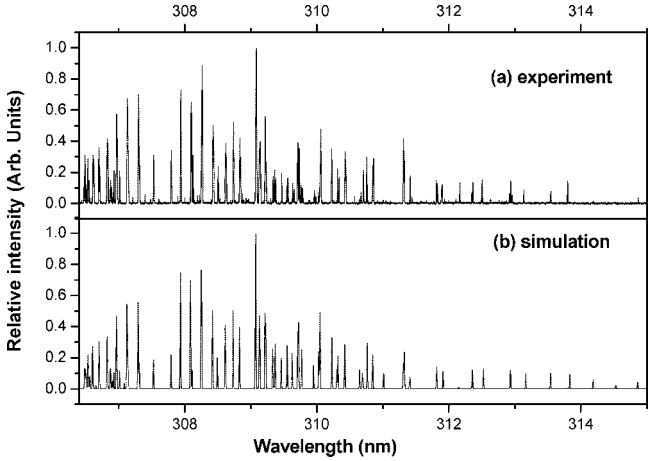

Figure 1. Comparison of the LIF excitation spectrum of the nascent OH ($A^2\Sigma^+$ ($v' = 0$) ← $X^2\Pi$ ($v'' = 0$)) photofragment following 289 nm photolysis of BAM: (a) experiment and (b) simulation.

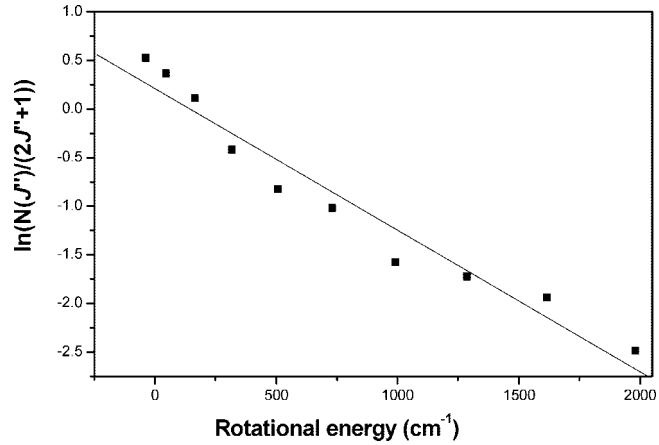

Figure 2. Boltzmann plot of the rotational energy distribution of the nascent OH fragment from the photodissociation of BAM at 289 nm. The solid line is the best fit to the data points and represents a rotational temperature of 594 K.

produce the frequency-doubled laser pulses, which were used for the probe laser pulses. Both the photolysis and the probe beams were counter propagated and softly focused on the center of the photolysis cell. The probe laser was delayed 15 ns with respect to the photolysis laser, which was controlled by a generator (SRS, DG535). This delay period was sufficient to separate the two laser pulses and was short enough to make collision effects negligible under the pressure (typically 200 mTorr) during the experiments.

The fluorescence of the OH fragment was collected by a photomultiplier tube (PMT, Hamamatsu CR161). A suitable narrow-band filter (310 nm, fwhm = 15 nm, $\%T_{310\ nm} = 30\%$) was placed in front of the PMT to cut off scattering from the photolysis laser and probe laser. The signal was gate-integrated by a boxcar (SRS, SR250), A/D converted by a homemade interface, and stored into a personal computer.

Benzoic acid (≥99.5%) was purchased from Shengyang Lianbang Chemicals Reagents Company and used without further purification. During the experiment, the sample was heated to 370 K; the helium carrier gas was bubbled through the sample, and the gas mixture was expanded into the photolysis cell. The benzoic acid was mostly monomer during the experiment, which was verified in our previous report.[25]

Results and Discussion

The formation of OH radicals was observed on excitation of BAM in the range of 280−294 nm. The measured OH LIF signal was found to be linearly dependent on the photolysis as well as probe laser powers, indicating that the photodissociation of BAM was a single-photon process and that the fluorescence was not saturated. Figure 1a shows the experimental LIF excitation spectrum of the nascent OH $A^2\Sigma^+$ ($v' = 0$) ← $X^2\Pi$ ($v'' = 0$) produced from BAM at 289 nm. The intensities of the observed LIF rotational lines were normalized with respect to the pressure in the photolysis cell, the energies of the probe laser, and photolysis laser. For assigning and analyzing the experimental LIF spectra, the experimental spectra were compared with the simulated OH excitation spectra. The intensities of the simulated fluorescence signal (I_F) are related to the populations of a ground rovibrational state N (J'', v'') by the expression:

$$I_F \propto \frac{N(J'', v'')q_{v'v''}S_{J'J''}f(\nu, \nu_0)}{(2J''+1)} \qquad (1)$$

where $q_{v'v''}$ are the known Franck−Condon factors for the OH $A-X$ transition;[29] $S_{J'J''}$ are the line strengths factor for the OH $A-X$ one-photon rotational transitions;[30] and $f(\nu, \nu_0) = \rho(\nu_0)\exp(-a(\nu-\nu_0)^2)$ is the laser intensity function. The simulated spectrum of OH (0, 0) band is plotted in Figure 1b. The experimental LIF excitation spectra at other photolysis wavelengths were also simulated.

The OH transitions were labeled following Hund's case (a). The P, Q, or R branches are for the cases of ΔJ or $\Delta N = -1$, 0, and 1, and the subscript 1 or 2 represents the different spin−orbit states $\Pi_{3/2}$ or $\Pi_{1/2}$, respectively. According to the parity selection rule (+ ↔ −), the Q branches only correspond to the Π^- state, while the P and R branches are attributed to the Π^+ state.

A. Rotational State Distribution. The OH rotational distributions at 280−294 nm photolysis of BAM are determined by analysis of the Q, P, and R branches from the $\Pi_{3/2}$ state or $\Pi_{1/2}$ state. On the basis of the normalized experimental data, the rotational state distribution could be characterized by a Boltzmann temperature. The equation of the Boltzmann population distribution is expressed as

$$\ln\frac{N(J'')}{(2J''+1)} = \frac{-\varepsilon(J'')hc}{kT_R} + \text{constant} \qquad (2)$$

A typical Boltzmann plot is shown in Figure 2. The solid line is the best fit to all of the points, and the rotational temperature at 289 nm is 594 ± 60 K. The rotational state distribution of the OH product is described reasonably well by the Boltzmann distribution, although the rotational populations deviate from Boltzmann distribution slightly at lower rotational quantum numbers J''. For all of the photolysis wavelengths, the rotational temperatures of OH are approximately 595 ± 60 K, where the error bar 60 is the maximum value of all of the error bars of rotational temperatures. The rotational state distributions of OH at 280 and 294 nm were also given in Figure 3. The rotation state distributions were peaked at $J'' = 3.5$ and extended to $J'' = 13.5$ at both wavelengths. The similar trend was also found at other wavelengths. Similar rotational state distributions of the OH fragments from the photolysis at different wavelengths indicate that the internal energy of OH does not change with different excited energies. This implies that the dissociation occurs from a repulsive state, or from a potential energy surface having a barrier, with the residual energy being distributed in the relative translation.

The probe laser was scanned in the range of OH $A^2\Sigma^+$ ($v' = 1$) ← $X^2\Pi$ ($v'' = 1$) transition at each photolysis wavelength,

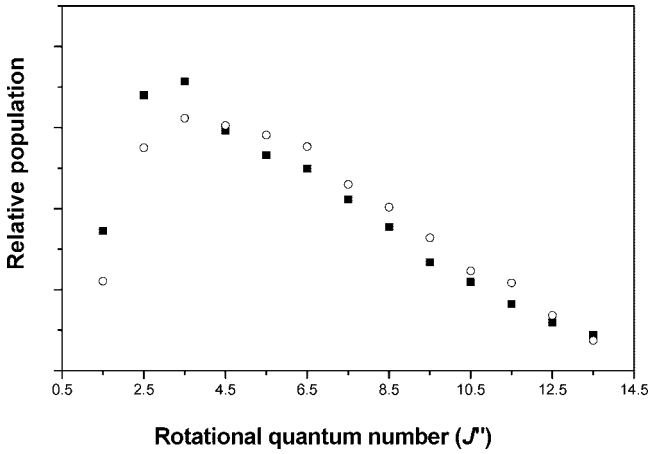

Figure 3. Rotational population distribution of OH fragments produced from the photodissociation of BAM at 280 and 294 nm, respectively. The filled squares represent the 280 nm and the circles represent the 294 nm.

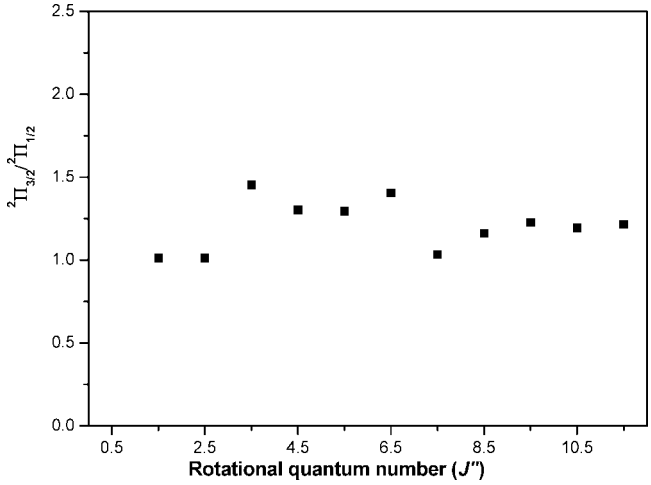

Figure 4. Spin−orbit ratios as a function of the rotational quantum number J'' for nascent OH $X^2\Pi$ ($v'' = 0$) from the photodissociation of BAM at 289 nm.

but no LIF signal was observed in the present experimental setup. Hence, the OH fragment was vibrationally cold from the photodissociation of BAM at 280−294 nm.

B. Spin−Orbit State Distribution and Λ-Doublet-State Distribution. The population of the $\Pi_{3/2}$ state (probed by P_1, R_1, and Q_1) to that of the $\Pi_{1/2}$ state (probed by P_2, R_2, and Q_2) is generally known as the F_1/F_2 ratio. The $\Pi_{3/2}/\Pi_{1/2}$ ratio measured at 289 nm is plotted versus the rotational quantum number J'' in Figure 4, and the averaged spin−orbit ratio for all photolysis wavelengths is calculated to be 1.2 ± 0.2. At each photolysis wavelength, the $\Pi_{3/2}$ level seems to be slightly more populated. The preferential population of $\Pi_{3/2}$ suggests a coupling between the initially prepared excited states with a nearby triplet state.[31]

The Λ-doublet ratio represents the orientation of the $p\pi$ lobe with respect to the OH rotating plane, denoted as Π^- (A″) and Π^+ (A′) state. In the Π^+ (A′) state, the $p\pi$ lobe lies in the plane of rotation, while in the Π^- (A″) state, the $p\pi$ lobe is perpendicular to the plane of rotation.[31] As mentioned above, the Q branches detect the OH fragment in the Π^- state, while R (and P) branches are due to the Π^+ state. Thus, the Λ-doublet ratio [Π^- (A″) /Π^+ (A′)] is obtained from Q/P or Q/R. In Figure 5, the Λ-doublet ratio for the $\Pi_{3/2}$ and $\Pi_{1/2}$ states, obtained from the Q/P ratios at 289 nm are shown with the function of

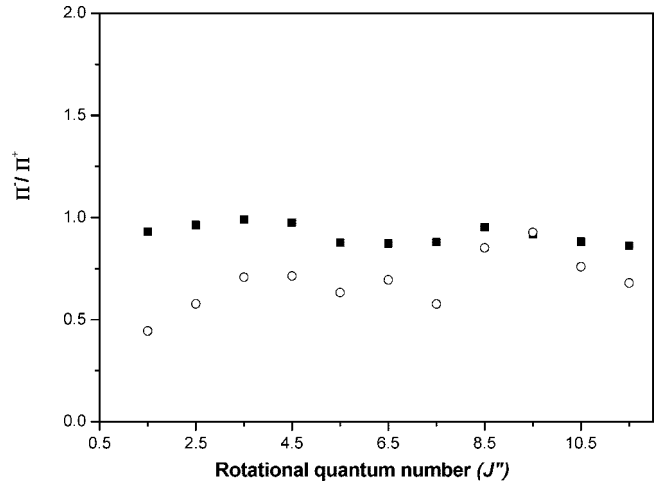

Figure 5. Λ-doublet ratios as a function of the rotational quantum number J'' for nascent OH $X^2\Pi$ ($v'' = 0$) from the photodissociation of BAM at 289 nm. The filled squares represent the $\Pi_{1/2}$ state and the circles represent the $\Pi_{3/2}$ state.

TABLE 1: Internal Energy of BAM Calculated with the B3LYP Method

	internal energy(kcal/mol) at different temperature			
basis set	370 K	350 K	320 K	298 K
6−31G(d, p)	6.65	6.08	5.06	4.46
6−311+G(d, p)	6.68	6.02	5.10	4.48
6−311++G(df, pd)	6.67	5.99	5.09	4.47
6−311G (2df, 2dp)	6.63	5.98	5.06	4.45

rotational quantum number J'', and the averaged Λ-doublet ratios of $\Pi_{3/2}$ and $\Pi_{1/2}$ states for all photolysis wavelengths are calculated to be 0.7 ± 0.2 and 0.9 ± 0.1, respectively. The distributions of the Π^+ state are slightly preferential than that of the Π^- state for all photolysis wavelengths, which suggests that the $p\pi$ electronic orbital of the OH radical is preferentially in its plane of rotation.

C. Estimating the Threshold for OH Production. On photoexcitation of BAM, two possible pathways are responsible for the OH formation. The first pathway is direct dissociation of the excited parent molecule C_6H_5COOH to form C_6H_5CO and OH; the second pathway involves C−C single bond cleavage resulting in C_6H_5 + COOH and a secondary decomposition of COOH through the C−OH bond dissociation to form OH and CO. On the basis of thermochemical data, the C−C bond and HO−CO bond cleavage were estimated to be endothermic by 105.2[32] and 36.0 kcal/mol,[33] respectively. Thus, the needed minimal energy for the second pathway to produce the OH fragment was 141.2 kcal/mol. The energy range of photolysis laser is from 96.92 to 102.1 kcal/mol. In the present experiment, the sample and the stainless-steel pipe were heated and maintained at 370 K, so the internal energy of BAM should be considered. The internal energies of BAM at different temperatures were calculated by ab initio calculations utilizing the Gaussian 03 program package.[34] The calculations were performed with the B3LYP theory, and using 6−31G (d, p), 6−311+G (d, p), 6−311+G (df, p), and 6−311G (2df, 2dp) basis sets respectively. The calculated results are listed in Table 1. As shown in Table 1, the values of the internal energies of BAM at a particular temperature, calculated by different basis sets, are approximately the same, indicating the effects of basis sets can be neglected. The internal energy of BAM was roughly estimated to be from 5.6 to 6.6 kcal/mol in our experiment

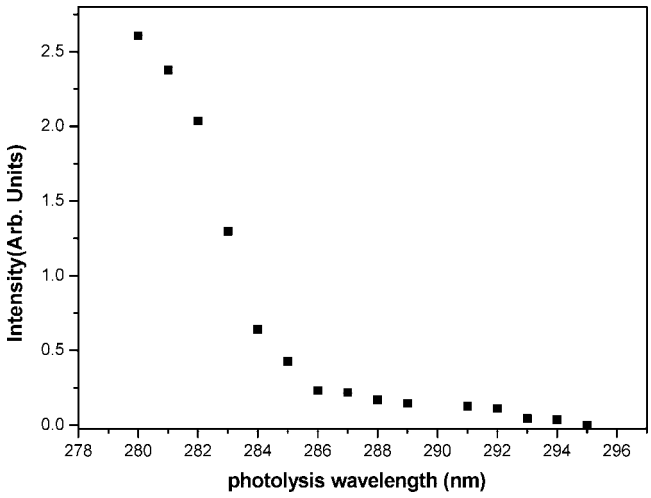

Figure 6. LIF intensities of OH Q_1 (3.5) rotational line from the photodissociation of BAM at different photolysis wavelength.

conditions, considering the deviation of the sample temperature in the photolysis region and the S_2 state electronic origin of BAM. So, the maximal total energy for photodissociation of BAM is 108.7 kcal/mol, which is not enough for the second path to form the OH product. However, the C−OH bond cleavage was predicted to be endothermic by 98.7 kcal/mol,[24] which is less than the total photodissociation energy. Therefore, the observed OH product in photodissociation of BAM in our experiment is due to the direct C−OH bond cleavage.

Establishment of the energy threshold for OH production from BAM is an essential ingredient to understand the dynamics of its photochemical process. We get the threshold for OH production from BAM by comparing the LIF intensity of Q_1 (3.5) rotational line at each photolysis wavelength. The LIF intensity of the Q_1 (3.5) rotational line at each photolysis wavelength is normalized with respect to pressure, intensities of photolysis, and probe laser. The LIF intensity of the Q_1 (3.5) rotational line with the function of photolysis wavelengths is plotted in Figure 6. The LIF intensity of the Q_1 (3.5) rotational line decreased rapidly from 280 to 286 nm and slowly from 286 to 295 nm. The LIF signal of the OH Q_1 (3.5) rotational line can be observed at 294 nm but not at 295 nm. It is reasonable to question that the lack of OH LIF signal at 295 nm is due to the reduction in absorption coefficients of BAM. We examined the UV absorption spectra of BAM[35] carefully, but the absorption efficient is almost the same at both 294 and 295 nm photolysis wavelengths. Actually, the LIF signal of OH vanished when the photolysis wavelength turned to 295 nm in our experiment. As we did not obtain the LIF signal of OH at the photolysis wavelength between 294−295 nm, thus, the 294 and 295 nm (97.25 and 96.92 kcal/mol) wavelengths are attributed to the upper and lower limit of the photodissociation threshold for OH production from BAM. By adding the internal energy 5.6−6.6 kcal/mol and by considering the deviation of the sample temperature in the photolysis region and the S_2 state electronic origin of BAM, the lower and upper limit of the photodissociation threshold for producing the OH radical from BAM are estimated to be 102.5 and 103.9 kcal/mol. Fang and co-workers[24] have predicted that C−OH bond cleavage of BAM to produce OH fragment occurs on photoexcitation at 270 nm (105.9 kcal/mol) or shorter wavelengths. Our estimated energy threshold is about 3 kcal/mol less than the calculated result, which indicates a good agreement between the calculated result and our experimental results.

One possible reason for absence of the LIF signal of OH at 295 nm is that a barrier for OH exit channel and the total photodissociation energy were not higher than the barrier for producing the OH fragment. The other possible reason for absence of the LIF signal of OH at 295 nm is that the BAM was excited to the S_1 state and not to the S_2 state. The electronic origin of the S_2 state is located at 35 924 cm^{-1} (102.7 kcal/mol).[20] By considering the lower limit of energy threshold, there exists the possibility that the total photodissociation energy at 295 nm was a little below the S_2 state. According to the calculated results,[24] the oscillator strength of the $S_0 \rightarrow S_2$ transition is 75 times larger than that for the $S_0 \rightarrow S_1$ absorption, implying that BAM is populated few to the S_1 state at 295 nm. Thus, the dissociation from the S_1 state or other lower states decayed from the S_1 state to produce OH would be negligible. This may be responsible for the absence of the LIF signal of OH at 295 nm. Which one is more reasonable between these two possible reasons is based on whether the height of barrier for producing the OH fragment is higher than the electronic origin of the S_2 state or not.

D. Dissociative State and Mechanism for Photodissociation of BAM. In the present experiment, by selecting the photolysis wavelength, we can get the information about not only the threshold but also the dissociative state for producing OH radical from photodissociation of BAM. In our previous experiment,[25] we have carried out the photodissociaton at 306−315 nm, but no LIF signal of OH was observed which indicated that the OH fragment could not be produced on the S_0 state. The calculated results[24] have shown that the S_1 and T_2 states were related to the production of OH. Relative to the S_0 zero level, the energy barriers were 107.1 and 102.3 kcal/mol for OH production from the S_1 and T_2 potential energy surfaces, respectively.[24] Considering the internal energy of BAM, if the photolysis wavelength is shorter than 284.5 nm (100.5 kcal/mol), the total energy of photolysis is above the barriers on the S_1 and T_2 states. Thus, BAM has the ability to pass the barriers on the S_1 and T_2 states to produce the OH radical. However, if the wavelength of the photolysis laser is longer than the 284.5 nm, the total energy of photolysis is below the barrier on the S_1 state but higher than the barrier on the T_2 state; the OH is produced only from the T_2 state. By comparing the state distribution of OH produced from different photodissociation energy, we can get the information about the dissociative state. The state distributions of OH at each photolysis wavelength were carefully analyzed, and we found that they are essentially of similar distribution, even compared to the state distribution of OH at 266 nm. Hence, the T_2 state is proposed to be the dissociative state for photodissociation of BAM at 280−294 nm.

Information on whether a molecule dissociates from a triplet potential energy surface can be obtained from the ratio of the spin−orbit states. A triplet dissociative state can change the spin−orbit ratio in the favor of the $\Pi_{3/2}$ state.[31] Actually, at each photolysis wavelength, the observed spin−orbit ratios show the slight preference for the $\Pi_{3/2}$ state of OH produced after photolysis of BAM.

Now we can get a picture of the photodissociation mechanism of BAM. The BAM was populated to the S_2 state when excited at 280−294 nm and then dissociated from the T_2 state. The T_2 state can be formed through two different ways. One is a direct way, through intersystem crossing from the S_2 state to the T_2 state. The other is an indirect way, which involves a three-surface intersection $S_1/T_1/T_2$ calculated by Fang and co-workers.[24] The three-surface intersection $S_1/T_1/T_2$ lied between

the T_1 and the S_1 states and successfully elucidates the photophysical process of BAM. So the indirect way involves relaxation of the prepared S_2 state of BAM to the S_1 state through internal conversion, which subsequently crosses to the T_2 state through three-surface intersection $S_1/T_1/T_2$.

Conclusion

In this study, the photodissociation dynamics of the BAM at 280−295 nm has been investigated. The averaged rotational temperature of OH radicals is 595 K for all of the photolysis wavelengths, and the OH fragments are vibrationally cold. The OH fragment is found to be slightly more populated in the $\Pi_{3/2}$ state compared with the $\Pi_{1/2}$ state, and the preferential population of the OH fragment in the Π^+ state is also observed at each photolysis wavelength. The dissociation takes place along the T_2 state potential energy surface, and the energy threshold for producing OH from BAM is estimated to be 102.5−103.9 kcal/mol. It is concluded that when BAM is excited at 280−294 nm, the initially prepared S_2 state undergoes direct and indirect transitions to the T_2 state and from where the molecule subsequently dissociates.

Acknowledgment. This work was financially supported by NKBRSF (2007CB815202), NSFC (20573110) and the knowledge innovation program of the Chinese academy of sciences (DICP R200603).

References and Notes

(1) Naik, P. D.; Upadhyaya, H. P.; Kumar, A.; Spare, A. V.; Mittal, J. P. *J. Photochem. Photobiol. C* **2003**, *3*, 165.
(2) Ni, C. K.; Lee, Y. T. *Int. Rev. Phys. Chem.* **2004**, *23*, 187.
(3) Han, K. L.; He, G. Z. *J. Photochem. Photobiol. C* **2007**, *8*, 55.
(4) Hunnicutt, S. S.; Waits, L. D.; Guest, J. A. *J. Phys. Chem.* **1989**, *93*, 5188.
(5) Hunnicutt, S. S.; Waits, L. D.; Guest, J. A. *J. Phys. Chem.* **1991**, *95*, 562.
(6) Kwon, H. T.; Shin, S. K.; Kim, S. K.; Kim, H. L.; Park, C. R. *J. Phys. Chem. A* **2001**, *105*, 6775.
(7) Naik, P. D.; Upadhyaya, H. P.; Kumar, A.; Spare, A. V.; Mittal, J. P. *Chem. Phys. Lett.* **2001**, *116*, 340.
(8) Arendt, M. F.; Browning, P. W.; Butler, L. J. *J. Chem. Phys.* **1995**, *103*, 5887.
(9) Kitchen, D. C.; Forde, N. R.; Butler, L. J. *J. Phys. Chem. A* **1997**, *101*, 6603.
(10) Owrutsky, J. C.; Baronavski, A. P. *J. Chem. Phys.* **1999**, *111*, 7329.
(11) Su, H. M.; Kong, F. N.; Fang, W. H.; Liu, R. Z. *J. Chem. Phys.* **2000**, *113*, 1891.
(12) Kumar, A.; Upadhyaya, H. P.; Naik, P. D. *J. Phys. Chem. A* **2004**, *108*, 6275.
(13) Dhanya, S.; Kumar, A.; Upadhyaya, H. P.; Naik, P. D.; Saini, R. D. *J. Chem. Phys.* **2003**, *118*, 10093.
(14) Pushpa, K. K.; Upadhyaya, H. P.; Kumar, A.; Naik, P. D.; Bajaj, P. N. *J. Chem. Phys.* **2004**, *120*, 6964.
(15) Upadhyaya, H. P.; Kumar, A.; Naik, P. D.; Sapre, A. V.; Mittal, J. P. *J. Chem. Phys.* **2002**, *117*, 10097.
(16) Kumar, A.; Upadhyaya, H. P.; Naik, P. D.; Maity, D. K.; Mittal, J. P. *J. Phys. Chem. A* **2002**, *106*, 11847.
(17) Kumar, A.; Naik, P. D. *Chem. Phys. Lett.* **2006**, *422*, 152.
(18) Baba, H.; Kitamura, M. *J. Mol. Spectrosc.* **1972**, *41*, 302.
(19) Kamei, S. I.; Abe, H.; Mikami, N.; Ito, M. *J. Phys. Chem.* **1985**, *89*, 3636.
(20) Meijer, G.; Vries, M. S.; Hunziker, H. E.; Wendt, H. E. *J. Phys. Chem.* **1990**, *94*, 4394.
(21) Bakker, J. M.; MacAleese, L.; Helden, G. V.; Meijer, G. *J. Chem. Phys.* **2003**, *119*, 11180. and references therein.
(22) Li, J.; Brill, T. B. *J. Phys. Chem. A* **2003**, *107*, 266.
(23) Ruelle, P. *J. Mol. Struct. (THEOCHEM)* **1987**, *8*, 158.
(24) Li, J.; Zhang, F.; Fang, W. H. *J. Phys. Chem. A* **2005**, *109*, 7718.
(25) Wei, Q.; Sun, J. L.; Yue, X. F.; Yin, H. M.; Han, K. L. *Chem. Phys. Lett.* **2007**, *448*, 11.
(26) Yin, H. M.; Sun, J. L.; Li, Y. M.; Han, K. L.; He, G. Z. *J. Chem. Phys.* **2003**, *118*, 8248.
(27) Li, Y. M.; Sun, J. L.; Han, K. L.; He, G. Z. *Chem. Phys. Lett.* **2006**, *421*, 232.
(28) Yue, X. F.; Sun, J. L.; Liu, Z. F.; Wei, Q.; Han, K. L. *Chem. Phys. Lett.* **2006**, *426*, 57.
(29) Luque, J.; Crosley, D. R. *J. Chem. Phys.* **1998**, *109*, 439.
(30) Kovacs, I. *Rotational Structure in the Spectra of Diatomic Molecule*; Adam Hilger Ltd.: London, 1969.
(31) Vasudev, R.; Zare, R. N.; Dixon, R. N. *J. Chem. Phys.* **1984**, *80*, 4863.
(32) (a) Feller, D.; Dixon, D. A.; Fransico, J. S. *J. Phys. Chem. A* **2003**, *107*, 1604. (b) Domalski, E. S.; Hearing, E. D. *J. Phys. Chem. Ref. Data* **1993**, *22*, 805–1159. (c) Baulch, D. L.; Cobos, C. J.; Cox, R. A.; Esser, C.; Frank, P.; Just, Th.; Kerr, J. A.; Pilling, M. J.; Troe, J.; Walker, R. W.; Warnatz, J. *J. Phys. Chem. Ref. Data* **1992**, *21*, 411. (d) Rui, M. B. D. S.; Jose, A. M.S. *J. Phys. Chem. Ref. Data* **1998**, *27*, 707.
(33) Benson, S. W. *Thermochemical Kinetics*; John Wiley and Sons: New York, 1968.
(34) Frish, M. J. et al. *Gausian 03*, Revision C.01; Gaussian Inc.: Pittsburgh, PA, 2003.
(35) Baum, J. C.; McClure, D. S. *J. Am. Chem. Soc.* **1979**, *101*, 2336.

JP711806U